# Motion of a Free-Settling Spherical Particle Driven by a Laser-Induced Bubble

Shengji Wu,[1] Zhigang Zuo,[1] Howard A. Stone,[2] and Shuhong Liu[1,*]
[1]State Key Laboratory of Hydroscience and Engineering, Department of Thermal Engineering, Tsinghua University, 100084 Beijing, China
[2]Department of Mechanical and Aerospace Engineering, Princeton University, Princeton, New Jersey 08544, USA
(Received 31 August 2016; published 25 August 2017)

We document experimentally four different interactions of a laser-induced bubble and a free-settling particle, with different combinations of the geometric and physical parameters of the system. Our force balance model shows that four nondimensional factors involving the particle radius $a$, the maximum bubble radius $R_{\max}$, the initial separation distance $l_0$ between the particle center and the bubble center, the fluid viscosity $\mu_f$, and the particle and fluid densities $\rho_p$ and $\rho_f$, respectively, in detail $l_0/R_{\max}$, $a/R_{\max}$, $\rho_p/\rho_f$, and $\mu^* = \mu_f T_c/\rho_f R_{\max}^2$, where $T_c = 0.915 R_{\max}\sqrt{\rho_f/(p_\infty - p_v)}$, influence the particle-bubble dynamics, and reasonably predict the maximum particle velocity and the limiting condition when the particle starts to "bounce off" the bubble during bubble growth. In particular, we also discover the high-speed ejection of the particle, and a cavity behind the particle, in cases when initially the particle is in very close proximity to the bubble. These observations offer new insights into the causal mechanism for the enhanced cavitation erosion in silt-laden water.

DOI: 10.1103/PhysRevLett.119.084501

Cavitation involves the physical processes of the "explosive" growth, or expansion, and the "implosive" collapse of vapor-filled bubbles, driven by tension in the liquid, or a local deposition of energy [1,2]. In hydrodynamic systems, the erosion of solid materials is among a number of undesirable effects promoted by cavitation [3], which can damage or impair the components of hydraulic machines [4]. The causal mechanism of the damaging power of cavitation is believed to be a consequence of the effects of high-speed microjets resulting from the asymmetric collapse of cavitation bubbles near solid boundaries [5–10].

Nevertheless, a much greater erosion rate has been observed when cavitation occurs in silt-laden water as compared with the sum of both cavitation and silt erosion considered separately [11]. Particle impingement on the surfaces of a specimen has been observed [12] and experiments have revealed that this enhancement is influenced by local flow conditions [13]. Despite a few analytical attempts [14], the micromechanism of this enhancement of erosion, in terms of the interactions between the cavitation bubbles and the silt particles, remains poorly understood and is the goal of this Letter. In fact, the coexistence of cavitation bubbles and solid particles is also found in other scenarios, e.g., ultrasonic cleaning [15], kidney stone fragmentation [16], and drug delivery by ultrasonic cavitation [17].

A number of studies have been dedicated to the dynamics of a cavitation bubble and a particle. For example, Soh *et al.* [18] used an electric spark to generate large bubbles in a water-filled tank under vacuum (100 kPa) in the vicinity of polyethylene particles, which were hanging from strings or resting on the boundary wall. No significant interactions were observed, quite likely because the particles were rather far away from the site of bubble formation. In addition, in a study of particulate transport in ultrasonic cleaning, Gonzalez-Avila *et al.* [19] used a focused laser beam to generate bubbles confined in a thin liquid gap where particles adhered to the boundaries. The authors observed large particle displacements only for nearby bubbles, strong particle rotation during bubble expansion, and an attractive force between the particle and the bubble during bubble collapse when the particle was close to the bubble. In order to experimentally observe the heterogeneous cavitation nucleation initiated by microparticles, Arora *et al.* [20] and Borkent *et al.* [21] focused strong tensile stress waves in a water flask in which were suspended polystyrene and acrylic polymer particles. A few instances where cavitation bubbles were generated on the polystyrene particle surface were found and the particle was then accelerated to speeds of ~40 m/s under the influence of bubble expansion. Recently, Poulain *et al.* [22] established an experimental setup, with bubbles generated by an electric spark and spherical particles slightly smaller than the bubbles attached to a thin steel rod. A pendulum-like movement of the rod in sync with the bubble growth and collapse was obtained. The terminal velocity of the particles was in the range mm/s, and varied in an inverse-fourth-power law with distance between the particle and the bubble. These studies provide valuable insight to the interaction between cavitation bubbles and particles. Here we report a systematic investigation to further

 

understand the mechanism of interaction of a bubble and a free-settling particle, with fewer restrictions and smaller disturbances to the motions of the particle and the cavitation bubble than in the studies indicated above, and we document new observations.

To simulate the dynamics of a particle near a cavitation bubble, we designed and fabricated an experimental setup, and for the first time study the interactions between a laser-induced vapor bubble and a free-settling particle. Furthermore, we develop a force balance model for the particle-bubble dynamics, predict the maximum particle velocity and distinguish the conditions for a single particle-bubble "bounce" (explained below), which are in agreement with the high-speed photographic observations. We also discover a high-speed ejection of the particle, and the appearance of a cavity behind the particle, in cases when initially the particle is in very close proximity to the bubble center.

We used a $Q$-switched pulsed ruby laser (wavelength: 694.3 nm, maximum pulse energy: 1.5 J, pulse length: 20–30 ns) to generate a cavitation bubble with maximum radius of about 2 mm in a quartz water chamber. The water chamber (140 mm × 140 mm × 150 mm) was filled with deionized and degassed water ($O_2$ concentration <2 ppm) and all experiments took place at room temperature.

Spherical particles of three different materials, polystyrene (PS, 1.05 g/cm$^3$), poly (methyl methacrylate) (PMMA, 1.18 g/cm$^3$), and $SiO_2$ (2.20 g/cm$^3$), were used in the experiments. The radii of the particles were $a = 100\ \mu\text{m} \sim 500\ \mu\text{m}$. We placed a particle into a long thin tube for precise positioning. Then we used a signal generator (Rigol DG2021A) to trigger a laser and a high-speed camera (Phantom V711) as sketched in Fig. 1. The motions of the particle and the bubble were recorded by the camera (at 210 526 frames/s with an exposure time of 1 $\mu$s) for subsequent analyses. A PVDF hydrophone (IACAS 070611) measured the time dependence of the shock waves produced by bubble generation and collapse, which determines the lifetime of the bubble.

For the convenience of depicting the system characteristics, we use three nondimensional parameters, $l/R_{\max}$, $a/R_{\max}$, and $\rho_p/\rho_f$, where $l(t)$ is the time dependent distance between the particle center and the bubble center

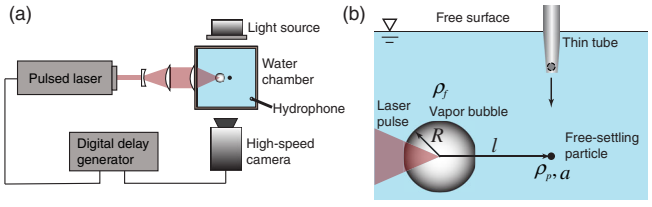


FIG. 1. Experimental configuration and notation. (a) Schematic of the experimental setup with a top view synchronized with the laser pulse. (b) Positioning of the free-settling particle near a laser-induced cavitation bubble.

(see Fig. 1), $l_0$ is the initial distance, $a$ is the radius of the particle, $R_{\max}$ is the maximum radius of the bubble, and $\rho_p$ and $\rho_f$ are, respectively, the density of the particle and water. A fourth nondimensional parameter $\mu^* = \mu_f T_c/\rho_f R_{\max}^2$, where $\mu_f$ is the fluid viscosity and $T_c$ is the Rayleigh collapse time of a bubble, will be introduced below.

Four typical sequences of particle motion induced by a nearby laser-induced bubble are presented in Fig. 2. In some of the events [Figs. 2(a)–2(b)], the particle oscillates in space about its original position, along the extended line between the centers of the bubble and the particle. The majority of the bubble surface undergoes symmetrical growth and collapse. As the relative particle size $a/R_{\max}$ varies (typically $R_{\max}$ is a few mm), the dynamics of the system becomes more complex with decreasing magnitude of the relative distance between the particle and the bubble $l_0/R_{\max}$. For example, a scenario when the particle "bounces off" the bubble is shown in Fig. 2(b), where we have chosen this wording to describe the process that the particle contacts the bubble surface and then "bounces back," from the reference of the relative motion of the particle against

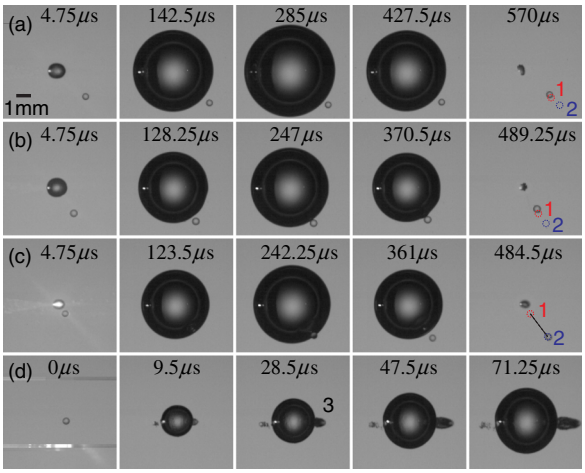


FIG. 2. Changing the relative position of the PMMA particle and the bubble. (a)–(d) High-speed recordings taken at 210 526 frames/s of the particle-bubble dynamics. Time $t = 0$ is the beginning of the last image frame before a laser-generated bubble forms. Here 1 and 2 indicate, respectively, the initial particle position and the furthest particle position from the bubble during a bubble's growth and collapse. The dashed line shows the trajectory of the particle. (a) The particle oscillates in sync with the bubble ($l_0/R_{\max} = 0.916$, $a/R_{\max} = 0.076$); the small asymmetry of the bubble in the first frame is due to the focusing of the laser beam. (b) The particle bounces off the bubble, with backward motion during bubble collapse ($l_0/R_{\max} = 0.780$, $a/R_{\max} = 0.088$). (c) The particle bounces off the bubble, with almost no backward motion ($l_0/R_{\max} = 0.262$, $a/R_{\max} = 0.090$). (d) The particle is ejected out of the bubble, with a cavity behind (indicated by 3 in the third frame, $l_0/R_{\max} = 0.111$, $a/R_{\max} = 0.074$). Scale bar is 1 mm. Details of the particle-bubble dynamics are available in the Supplemental Material [23].

the bubble surface. In Fig. 2(b), the bubble approaches and appears to deform in the neighborhood of the particle. Then the particle appears to contact the bubble surface when the bubble is near its maximum radius, and the bubble surface temporarily extrudes into a cusp shape when the particle bounces off the bubble while the bubble is shrinking. In contrast, in Fig. 2(c), the particle-bubble contact happens when the bubble is rapidly growing and the bounce and cusp shape occurs when the bubble is near the maximum radius. A traveling surface wave is observed along the bubble surface in Fig. 2(c) when the particle is slightly out of the focusing plane of the camera. With a very small $l_0/R_{\max}$, the particle is ejected from the bubble with a maximum velocity of over 60 m/s and a cavity immediately forms behind the particle [Fig. 2(d)]. In contrast to previous studies showing rapid particle movements when bubbles grow directly on a particle [20,21], here we have documented that a free-settling particle can be rapidly accelerated because of the growth of a nearby bubble. We have also performed additional experiments (see Ref. [23]) to distinguish bubble growth directly on a particle from plasma generation and bubble growth a small distance from the particle, and our general conclusions remain. Also we note that heating of the particle by a hot vapor bubble nearby to achieve the boiling temperature is estimated to be 1 ms, which is much longer than the time scale shown in Fig. 2(d).

Similar dynamics occur with other particles of different densities. In particular, we have taken high-speed recordings of the cases with $a/R_{\max}$ ranging from 0.02 to 0.20, and $\rho_p/\rho_f = 1.05$, 1.18 and 2.20, several of which are reported in Ref. [23].

The system of interest contains a free-settling particle of radius $a$, and a laser-induced cavitation bubble with radius $R(t)$. The settling velocity of the particle can be evaluated from the correlation $C_d = 24/\mathrm{Re}(1 + 0.15\mathrm{Re}^{0.687})$, where Re is the particle Reynolds number [26]. Considering the short observation time window (500 $\mu$s), the particle displacement due to the gravitational force is only about 30 $\mu$m. Thus, we neglect gravitational sedimentation of the particle during the time of the particle-bubble interaction. Because $a/R_{\max} \ll 1$, the influence of the particle on the flow field around the bubble is neglected. In addition, consistent with the experimental observations, one-dimensional motions of the bubble and the particle are assumed. Next we propose a force balance model to explain the particle-bubble dynamics.

Neglecting the Basset history force and buoyancy, then a force balance on the particle gives the equation of motion of the particle as [16,21,27]

$$\frac{d^2\lambda}{dT^{*2}} = \frac{\frac{3C_d}{4\gamma}|u_f^* - u_p^*|(u_f^* - u_p^*) + 3\frac{Du_f^*}{DT^*}}{(1 + 2\frac{\rho_p}{\rho_f})}, \qquad (1)$$

where $T^* = t/T_c$, $\gamma = a/R_{\max}$, $\lambda = l/R_{\max}$, $u_f^* = u_f/(R_{\max}/T_c)$, and $u_p^* = u_p/(R_{\max}/T_c)$. $T_c = 0.915R_{\max}\sqrt{\rho_f/(p_\infty - p_v)}$ is the Rayleigh time of a spherical cavitation bubble and $D/Dt$ is the material derivative. Here we have used $R_{\max}$ as a parameter since it is easily measured. In $C_d$, another nondimensional parameter, $\mu^* = \mu_f T_c/\rho_f R_{\max}^2$, appears. The drag force is important for small particles when $\mu^*$ is comparable to $\gamma^2$. In our experiments, $\mu^*$ remains nearly constant ($3.0 \times 10^{-5}$).

The motion of the particle is dependent on the bubble dynamics. Although the formation mechanism of a bubble by a laser is rather complex [28–30], the majority of the time evolution of the radius of a laser-induced bubble follows a symmetric curve for growth and collapse [31,32]. Thus, we can model the bubble dynamics for $R(t)$ with the approximate formula of Obreschkow *et al.* [33]

$$\frac{R}{R_{\max}} = \left[1 - \left(\frac{t}{T_c} - 1\right)^2\right]^{\frac{2}{5}}. \qquad (2)$$

We verified with our experiments that Eq. (2) can describe approximately one period of growth and collapse of the laser-induced cavitation bubble.

We solved Eqs. (1) and (2) numerically using as initial conditions $T_0^* = 10^{-6}$, $\lambda(T_0^*) = l_0/R_{\max}$, $(d\lambda/dT^*)_{T^*=T_0^*} = 0$. Two examples are presented in Figs. 3(a) and 3(b) where we report the bubble growth in time and the corresponding motion of the particle. Larger particle velocity is achieved with smaller initial distance between the particle and bubble centers [Fig. 3(c)]. The nondimensional maximum particle velocity $u_{p,\max}^*$ happens in the very early time of the bubble growth, before the particle touches the bubble. Our model shows that $a/R_{\max}$ hardly affects the value of $u_{p,\max}^*$, demonstrating that the effects due to the liquid acceleration ($Du_f^*/DT^*$) play a key role in the acceleration of the particle, especially in the initial stage. The model also predicts the same order of magnitude of the particle velocity as in the case shown in Fig. 2(d), with a very small $l_0/R_{\max}$. For example, a typical speed of the bubble surface $R_{\max}/T_c$, which indicates the magnitude of the particle speed, is approximately 10 m/s.

To evaluate the limiting condition when the particle starts to bounce off the bubble during bubble growth, we derive a maximum $l_0/R_{\max}$ when $l/R_{\max} = R/R_{\max} + a/R_{\max}$. The results of $l_0^{\mathrm{limit}}/R_{\max}$ at $\mu^* = 3.0 \times 10^{-5}$ and different $\rho_p/\rho_f$ and $a/R_{\max}$ are shown in Fig. 4. They are in good agreement with the experiments. The limiting value $l_0^{\mathrm{limit}}/R_{\max}$ when the particle starts to bounce off the bubble increases with an increase of $a/R_{\max}$ and $\rho_p/\rho_f$.

We can draw several conclusions based on Eqs. (1) and (2). Since $\mu^* \ll 1$, the drag force only plays a significant role for $\gamma = a/R_{\max} \lesssim \sqrt{\mu^*}$. $\mu^*$ does not impact significantly the maximum speeds to which the particle is accelerated, and even for small $a/R_{\max}$, it is not important

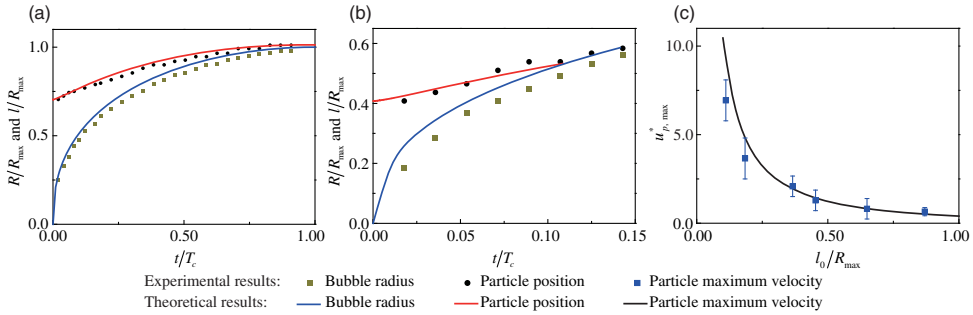


FIG. 3. (a)–(b) Comparison between analytical and experimental particle-bubble dynamics by plotting the bubble radius and PMMA particle position as a function of time. (a) $l_0/R_{max} = 0.705$, $a/R_{max} = 0.031$, (b) $l_0/R_{max} = 0.408$, $a/R_{max} = 0.051$, (c) influence of $l_0/R_{max}$ on $u^*_{p,max}$, $u^*_{p,max} = u_{p,max}/(R_{max}/T_c)$. In (a) and (b), errors bars are comparable to the size of the data points.

at early times. However, the influence of the drag force becomes significant in the cases of the limiting condition, since it appears at a much later time after the particle achieves its maximum speed.

In cases of particle-bubble bouncing, the particle either touches the bubble surface, forming a three-phase contact, or penetrates the bubble. The relative deceleration of the particle and bubble then results in reentrance of the particle back into water. We believe that the vapor cusp and the cavity behind the particle [Fig. 2(d)] we documented, with the typical Weber number $W = \rho_f u_{rs}^2 a/\sigma$, where $u_{rs}$ and $\sigma$ are, respectively, the relative velocity between the particle and the bubble surface at separation and the water surface tension (Fig. 5), is similar to the quasistatic and surface seal impact cavities that occur when a particle impacts the surface of a water bath [34,35]. Note that the vapor cusp remains at $W$ up to 70, which differs from values less than 10 in the water entry problems of small spheres, possibly due to a larger difficulty in maintaining an elongated cavity because of the rapid condensation of the vapor. According to the unsteady Bernoulli equation [36], a vapor cavity is also possible due to the high-speed movement of the particle, which is accelerated by the bubble.

In conclusion, we carried out experimental studies on the dynamics of a laser-induced bubble and a free-settling particle, which had not been studied previously, and discovered four different behaviors. Also, we establish a force balance model to account for the bubble and particle dynamics. Results show that the nondimensional parameters $l_0/R_{max}$, $a/R_{max}$, $\rho_p/\rho_f$, and $\mu^*$ influence the particle-bubble dynamics. The maximum particle velocity and the conditions of single particle-bubble bounce have been reasonably predicted.

In cases when the particle is initially in very close proximity to the bubble center, we also discover the high-speed ejection of the particle, and the formation of a cavity behind the particle. The maximum particle velocity reached over 60 m/s, which is enough to induce plastic deformation of a stainless steel plate [37]. The fact that a similar phenomenon of high-speed particle ejections occurs with a system of tension-generated bubbles and suspended particles [20,21] suggests that the dynamics described here may serve as one of the causal mechanisms for the enhanced cavitation erosion in silt-laden water.

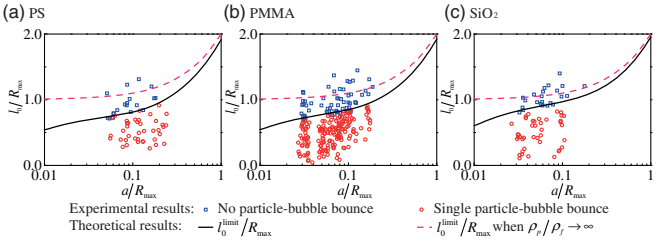


FIG. 4. Limiting condition when the particle starts to bounce off the bubble during bubble growth, as a function of $l_0/R_{max}$ and $a/R_{max}$, at $\mu_f T_c/\rho_f R_{max}^2 = 3.0 \times 10^{-5}$. (a) PS particle ($\rho_p/\rho_f = 1.05$), (b) PMMA particle ($\rho_p/\rho_f = 1.18$), (c) $SiO_2$ particle ($\rho_p/\rho_f = 2.20$). The solid and dashed lines represent $l_0^{limit}/R_{max}$ derived from the numerical solutions of Eqs. (1) and (2). Slightly different curves are found with different $\rho_p/\rho_f$.

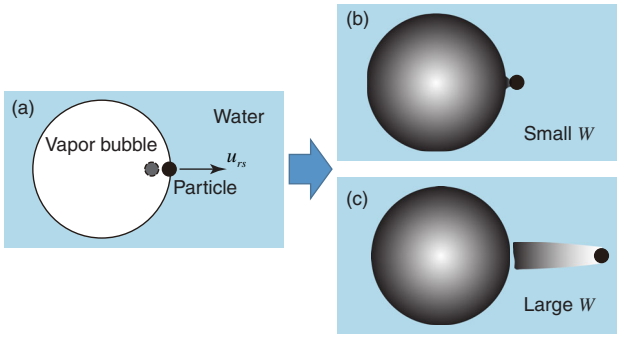


FIG. 5. Schematic of a particle re-entering water. (a) Particle inside a bubble, or on the bubble surface (three-phase contact). (b) Cusp-shaped quasistatic impact cavity behind a particle at small $W$. (c) Surface seal impact cavity behind a particle at large $W$.

The authors gratefully acknowledge inspiring discussions with Detlef Lohse, Qiang Yao, Chao Sun, and Shuiqing Li. The work was supported by the National Natural Science Foundation of China (No. 51476083) and the State Key Laboratory of Hydroscience and Engineering (No. sklhse-2015-E-02). H. A. S. is grateful to the Department of Thermal Engineering at Tsinghua University for a chair professorship.

*Corresponding author.
liushuhong@mail.tsinghua.edu.cn

[1] F. R. Young, *Cavitation* (World Scientific, Singapore, 1999).
[2] *Cavitation and Inhomogeneities in Underwater Acoustics: Proceedings of the First International Conference, Göttingen, Fed. Rep. of Germany, July 9-11, 1979*, edited by W. Lauterborn (Springer-Verlag, Berlin, 1980).
[3] A. Karimi and J. L. Martin, Int. Met. Rev. **31**, 1 (1986).
[4] S. C. Li, *Cavitation of Hydraulic Machinery* (Imperial College Press, London, 2000).
[5] J. R. Blake, B. B. Taib, and G. Doherty, J. Fluid Mech. **170**, 479 (1986).
[6] J. R. Blake and D. C. Gibson, Annu. Rev. Fluid Mech. **19**, 99 (1987).
[7] A. Vogel, W. Lauterborn, and R. Timm, J. Fluid Mech. **206**, 299 (1989).
[8] A. Philipp and W. Lauterborn, J. Fluid Mech. **361**, 75 (1998).
[9] Y. Tomita, P. B. Robinson, R. P. Tong, and J. R. Blake, J. Fluid Mech. **466**, 259 (2002).
[10] E. Brujan and Y. Matsumoto, Microfluid. Nanofluid. **13**, 957 (2012).
[11] V. I. Karelin and C. Duan, *Abrasive Erosion and Corrosion of Hydraulic Machinery* (Imperial College Press, London, 2002).
[12] H. Y. Jin, F. Z. Zheng, and S. Y. Li, Wear **112**, 199 (1986).
[13] J. Sato, K. Usami, T. Okamura, and S. Tanaba, ASME-Publications-FED **136**, 65 (1993).
[14] S. C. Li, Wear **260**, 1145 (2006).
[15] D. Krefting, R. Mettin, and W. Lauterborn, Ultrason. Sonochem. **11**, 119 (2004).
[16] J. E. Lingeman, J. McAteer, E. Gnessin, and A. Evanm, Nat. Rev. Urol. **6**, 660 (2009).
[17] C. Coussios and R. A. Roy, Annu. Rev. Fluid Mech. **40**, 395 (2008).
[18] W. K. Soh and B. Willis, Exp. Therm. Fluid. Sci. **27**, 537 (2003).
[19] S. R. Gonzalez-Avila, X. Huang, P. A. Quinto-Su, T. Wu, and C. D. Ohl, Phys. Rev. Lett. **107**, 074503 (2011).
[20] M. Arora, C. D. Ohl, and K. A. Mørch, Phys. Rev. Lett. **92**, 174501 (2004).
[21] B. M. Borkent, M. Arora, C. D. Ohl, N. D. Jong, M. Versluis, D. Lohse, K. A. Mørch, E. Klaseboer, and B. C. Khoo, J. Fluid Mech. **610**, 157 (2008).
[22] S. Poulain, G. Guenoun, S. Gart, W. Crowe, and S. Jung, Phys. Rev. Lett. **114**, 214501 (2015).
[23] See Supplemental Material at http://link.aps.org/supplemental/10.1103/PhysRevLett.119.084501 for the high speed videos of the interactions between a particle and a laser-induced bubble, a discussion on the effect of $\mu^*$ on the limiting condition, a comparison between bubble growth directly on a particle from plasma generation and at a small distance from the particle, and a discussion on the potential of heating of the particle by hot vapor, which includes Refs. [24,25].
[24] A. Vogel, S. Busch, and U. Parlitz, J. Acoust. Soc. Am. **100**, 148 (1996).
[25] H. S. Carslaw and J. C. Jaeger, *Conduction of Heat in Solids*, 2nd ed. (Clarendon Press, Oxford, 1959).
[26] L. Schiller and Z. Naumann, VD.I. Zeitung **77**, 318 (1935).
[27] J. Franc and J. Michel, *Fundamentals of Cavitation* (Springer Science & Business Media, 2006).
[28] I. Akhatov, N. Vakhitova, A. Topolnikov, K. Zakirov, B. Wolfrum, T. Kurz, O. Lindau, R. Mettin, and W. Lauterborn, Exp. Therm. Fluid. Sci. **26**, 731 (2002).
[29] K. Byun and H. Kwak, Jpn. J. Appl. Phys. **43**, 621 (2004).
[30] A. Prosperetti, Annu. Rev. Fluid Mech. **49**, 221 (2017).
[31] T. Sato, M. Tinguely, M. Oizumi, and M. Farhat, Appl. Phys. Lett. **102**, 074105 (2013).
[32] Y. Tomita, M. Tsubota, K. Nagane, and N. An-naka, J. Appl. Phys. **88**, 5993 (2000).
[33] D. Obreschkow, M. Bruderer, and M. Farhat, Phys. Rev. E **85**, 066303 (2012).
[34] J. M. Aristoff and J. W. Bush, J. Fluid Mech. **619**, 45 (2009).
[35] D. G. Lee and H. Y. Kim, Phys. Fluids **23**, 072104 (2011).
[36] M. Versluis, B. Schmitz, A. von der Heydt, and D. Lohse, Science **289**, 2114 (2000).
[37] G. P. Tilly, Wear **23**, 87 (1973).